Int. J. Multiphase Flow Vol. 10, No. 5, pp. 585–597, 1984
Printed in the U.S.A.

0301-9322/84 $3.00 + .00

FLOODING AND UPWARD FILM FLOW IN TUBES—I

EXPERIMENTAL STUDIES

A. E. DUKLER, L. SMITH and A. CHOPRA
Chemical Engineering Department, University of Houston, Houston, TX 77004, U.S.A.

(*Received* 1 *January* 1982; *in revised form* 18 *October* 1983)

Abstract—New data are presented on the details of the flooding process and upward film flow including film and entrainment flow rates, film structure, pressure drop, as well as interfacial and wall shear. These data are used to explore the mechanism of flooding and upward film flow in part II.

INTRODUCTION

Flow reversal or flooding in falling film systems has been a subject of experimental study for over 40 years. In the process industries the problem is of importance for vertical tube condensers where the vapor enters from the bottom and the condensed liquid falls countercurrent to the rising vapor. Flow reversal results in undesirable liquid carry over. Also of interest is the case of falling film chemical reactors or absorbers with counterflow of gas where carry over is undesirable. Perhaps the most common counterflow situation where flooding is important is in packed towers. In such systems the conditions of loading and flooding have been identified. Loading takes place as the gas rate is increased and to the point where the pressure drop across the packed bed increases sharply. The flooding point is the condition at which liquid carry up or flow reversal takes place. Gazely (1948) identified the loading point as the condition at which the liquid films which irrigate the packing begin to display wavy surfaces. The flooding point is described as the conditions where the waves grow sufficiently to bridge the packing free space at any cross section and thus block the flow of gas.

Predicting flow reversal of liquid films is particularly important for the conditions of a loss of coolant accident in pressurized water reactors. If a reactor depressurizes due to a pipe break, vaporization takes place and the reactor core, normally covered by water, can become exposed to steam. Even though the reactor is automatically shut down and fission stops, it is necessary to remove the heat generated by the decay of fission products in the fuel. This decay heat is sufficient to melt the reactor core in a matter of seconds if heat transfer effectiveness is impaired due to the absence of water. For this reason standby emergency cooling water is automatically injected into the reactor on loss of pressure. This water enters in an annulus counter to upflow of steam generated by the flashing water. The injected stream will reach the reactor core and cool the fuel rods only if the conditions do not exceed that for flooding. In another configuration cooling water is sprayed directly on to the top section of the fuel rods. Water must flow down the rods and into the core in order to effect cooling. However, if the upward steam flow causes flooding, the film will not penetrate the core and the cooling will not take place. This process of cooling water injection is an exceedingly complex one involving unsteady state flow conditions, condensation of the steam as a result of quenching by the cold water, flashing of input water due to hot walls, and the condition of pressure pulses and merging streams.

Empirical correlations have been constructed to predict the condition of flooding and flow reversal once experimental data have been obtained. However, no published

correlations have been successful in accounting for varying equipment size, configuration of inlet and outlet piping and operating pressure and temperature. The reason for this is clear. The physical mechanisms by which the process of flooding and reversal takes place are not understood even for the simplest case of a steady isothermal falling film with counter gas flow in a tube without phase change.

The experimental and analytical approaches to flooding that have appeared in the published literature and in reports were reviewed by Dukler & Smith (1977) and Tien & Liu (1979). In no case have the details of the flooding process been explored experimentally with the objective of uncovering the mechanisms which underlie the phenomenon. Probably because of this lack of understanding, no models have appeared which are fully satisfactory in predicting the process.

It is the purpose of the first of these papers to present the results of an experimental study of the *details* of the flooding/flow reversal process. This is followed by part II in which certain speculations on mechanism are put forward.

EXPERIMENTAL EQUIPMENT AND MEASURING SYSTEM

The experimental system was designed to permit the accurate measurement of a series of parameters considered important to exploring the mechanism of the flooding/flow reversal process in a vertical tube. The particular arrangement chosen was one for which the liquid feed was introduced at a location between the top and bottom of the column. It was the objective to be able to measure the manner in which the liquid distributed, that is, the amount flowing downward as a film below the feed W_D, that flowing upward as a film W_U and flowing upward as entrained drops W_E. In addition, the system was designed to make possible the measurement and simultaneous recording to time varying pressure $p(t)$ and film thickness $\delta(t)$, at up to four locations along the test section. Because there is a general belief that flooding results are dependent on the configuration of the test section and loop used, we will provide details to a degree more than usual.

Test sections

Three test section configurations were used for the series of measurement reported here. These are illustrated in figure 1. In all cases the sections were made of transparent Plexiglas pipe with 5.08 cm i.d. Various lengths were fitted together with special flanges machined to ensure smooth continuity of the inner surfaces at the joints. The liquid feed section consisted of a porous sinter whose inside diameter was carefully matched to the inside diameter of the pipe. Liquid falling below the feed was separated from incoming air at the bottom by the use of a flared section of pipe. A similar device was used at the top to separate the liquid or the film flowing upward from the gas and entrained droplets rising up the column. In configuration III a porous sinter located near the top was used to remove part of the liquid flowing upward as a film with the remainder being removed through the flare section and separator. The letters A–D in figure 1 designate the location of measuring stations where time varying data on film thickness and pressure could be obtained as discussed below. The dimensional arrays for these three configurations are shown in some detail in figure 1.

Configuration I was used exclusively for the measurement of pressure drop, W_U, W_D and W_E. In configuration II three of the four measuring stations were located below the feed and the focus of the measurement was on the film flow below the feed. In test section configuration III the feed sinter was located at the bottom, all four stations were located above the feed and the focus was on the characteristics of the rising film.

Flow loop

A schematic diagram of the flow loop appears in figure 2. Air is supplied from a rotary

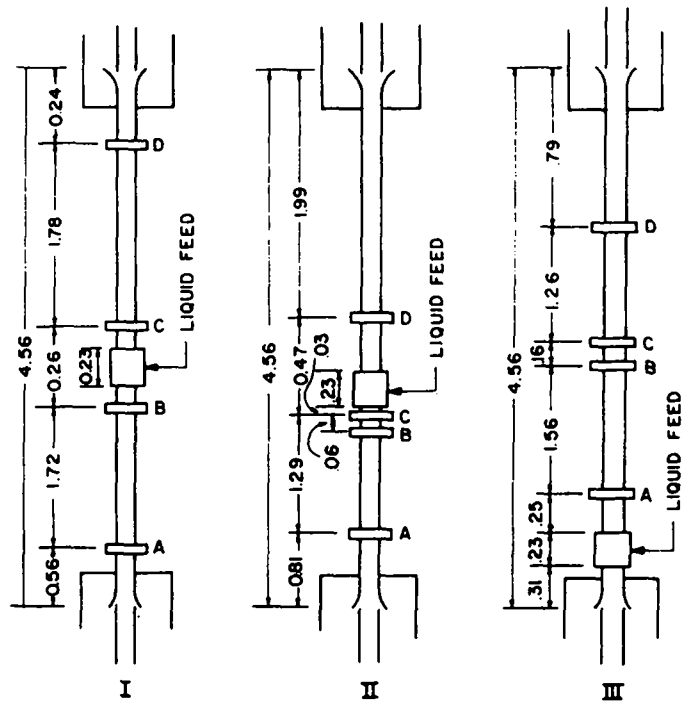

Figure 1. Three configurations of the test section (all dimensions meters).

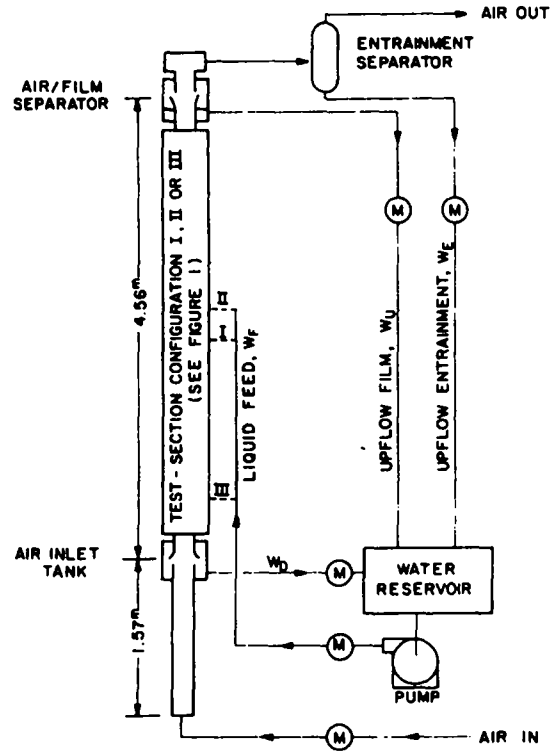

Figure 2. Schematic diagram of flow loop (Ⓜ indicates metered flow).

compressor through a straight entry length 5.08 cm i.d. and 1.57 m long which is axially aligned with the test section. Water flowing down as a film is separated from the rising air in the air inlet tank as shown using a flared connection on the bottom of the test section. This tank controls the water level to maintain a hydrostatic seal and passes the water flowing down to the reservoir. The rising liquid film enters an air/film separator tank at the top of the system. As in the air inlet tank at the bottom, a liquid level is automically

maintained in the tank and the film flow passes to the water reservoir. Air containing entrained drops flows to a centrifugal separator where the entrained liquid is removed. Water from the reservoir is supplied to the entry porous sinter by a centrifugal pump. As indicated on the diagram, in addition to metering the liquid and air feeds, W_D, W_U and W_E are measured.

Measuring stations

Two phase flow is an inherently time varying process with strong stochastic characteristics. As a result to the measurement of time averaging data is insufficient to provide insights into mechanisms. For this reason the measurements of pressure and film thickness are collected as time dependent variables. In this case the procedure is to transduce all measurements to analog voltage outputs and record these signals on a high accuracy multichannel tape recorder. The data are then processed through an analog to digital conversion system and the digital data are then processed using specialized software written for this purpose.

Figure 3 shows the measuring station. The system is described in detail by Chu & Dukler (1974). Film thickness is measured by an electrical conductance technique where the electrodes are flush with the wall and closely spaced. The technique depends on the fact that the conductance of a liquid film covering fixed electrodes is proportional to the thickness of the film as well as its temperature and salinity. The effects of temperature and

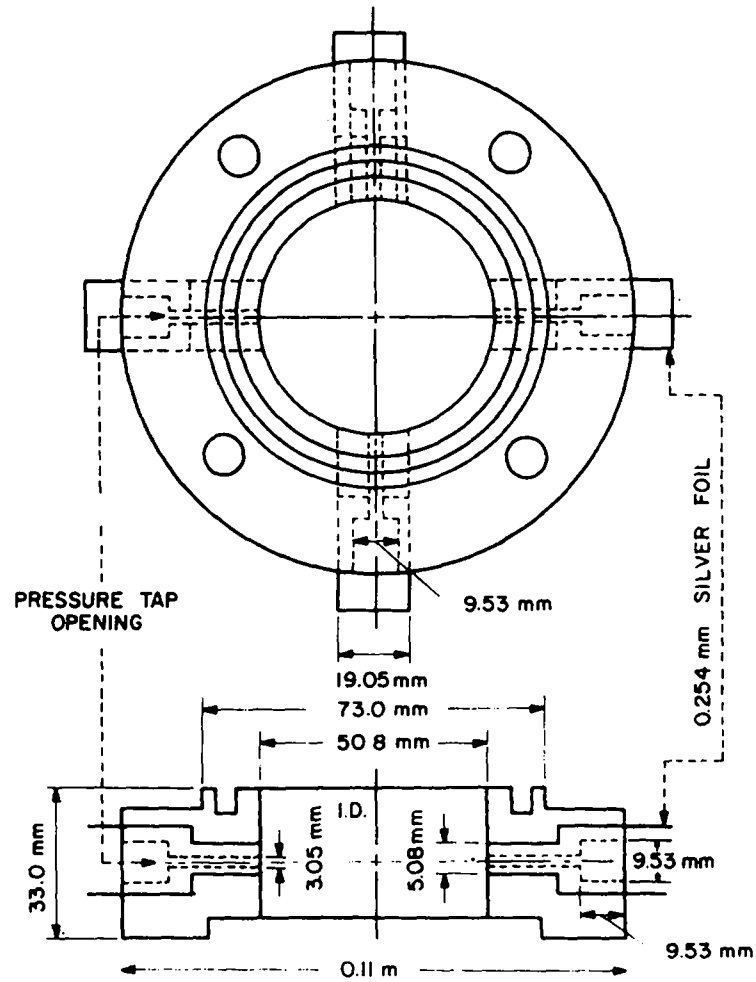

Figure 3. Measuring station.

salinity can be eliminated by continuously measuring the conductivity in a cell of fixed dimensions. The system was calibrated outside the test section by inserting a series of cylindrical plugs into the measuring station, each having an annular gap of known size. The calibration data was fit with a polynomial and the resulting relation between output voltage and film thickness incorporated into the software used to process the data.

Time varying pressure data were obtained through a small pressure tap located between the electrode pairs. Statham pressure transducers were mounted directly on the measuring station and the connecting space filled with water. Output from the transducers were amplified, the d.c. level subtracted using precision variable resistors and the resulting fluctuations further amplified for recording.

Details as to the individual units of equipment measurement techniques, test procedures, estimated measurement error and software have been reported (Chopra 1982; Smith 1983). These theses also contain complete tabulations of experimental data. All measurements were made with the system discharge at atmospheric pressure.

EXPERIMENTAL MEASUREMENTS

Liquid distribution

Data for liquid downflow W_D, flow upward as a film W_U, and upflow as entrainment W_E, appear in figures 4–6. Figure 4 shows that the downflow, or flooding curve, is independent of feed rate and of feed entry location. W_U and W_E are likewise feed location independent. It is of interest to note that the gas rate at which flooding occurs for each liquid feed rate W_F, is identically that rate where entrainment is first detected. It remains to determine if the entrainment is the mechanism of the flooding process or the result of flooding by another mechanism.

Pressure gradient

The mean (time average) pressure gradient measured both above and below the feed

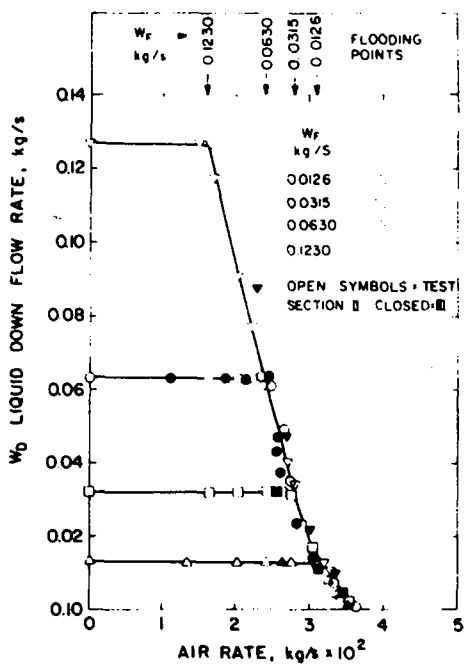

Figure 4. Down flow rates.

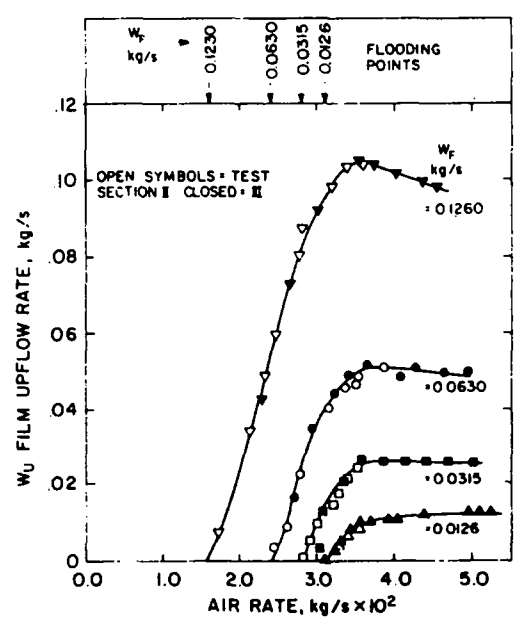

Figure 5. Film upflow rate.

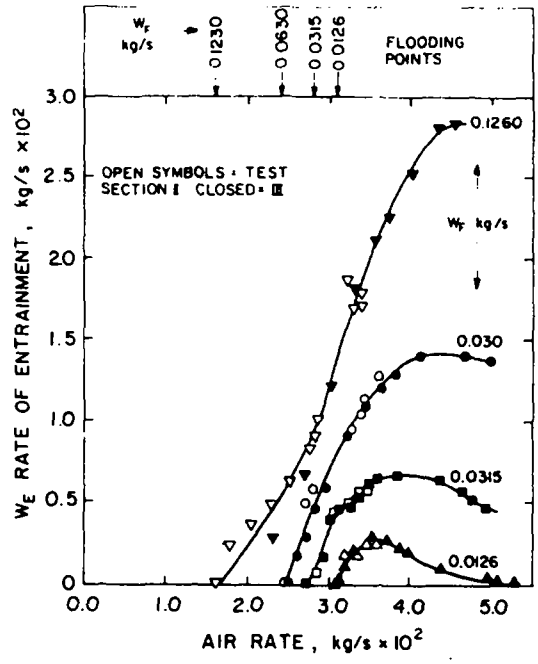

Figure 6. Rates of upflow by entrainment.

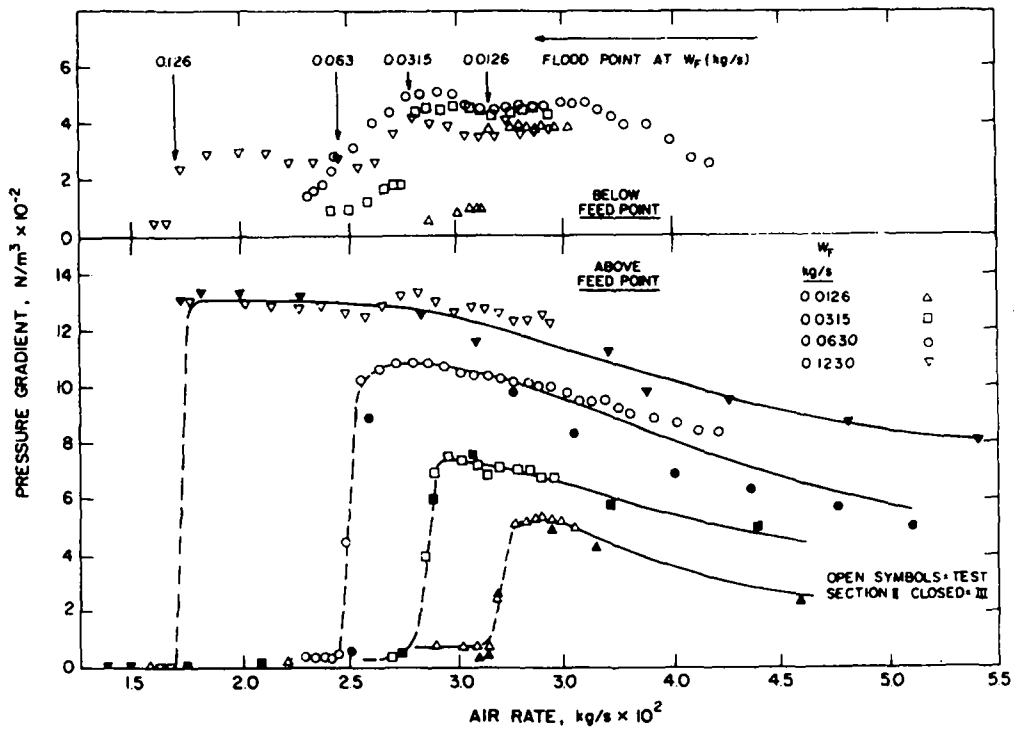

Figure 7. Pressure gradient above and below the feed for the flooding process.

is displayed in figure 7. The occurrence of flooding as evidenced by the data in figure 4 coincides quite precisely with a step increase in pressure gradient both above and below the feed. In the case of $W_F = 0.216$ kg/s, the system below the feed experiences two changes in gradient.

The time series were analyzed to obtain the RMS fluctuation in the pressure gradient and these are displayed for both above and below the feed in figure 8. It is apparent that the initiation of flooding is accompanied by a sharp increase in the level of fluctuation in

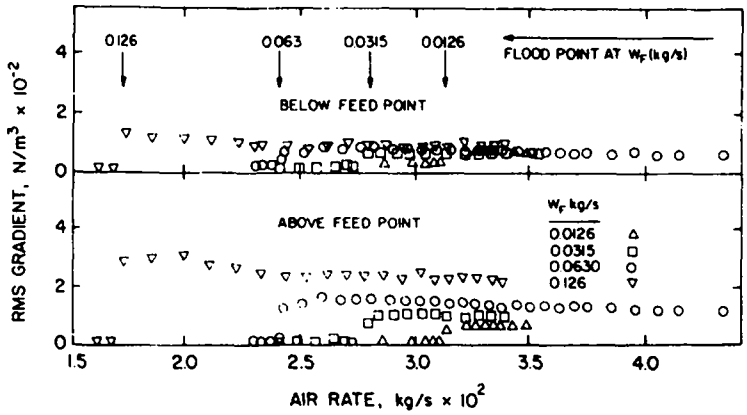

Figure 8. RMS fluctuation in the pressure gradient.

pressure gradient as well as in its mean value both above and below the feed. This implies a sharp increase in the level of fluctuation in interfacial shear stress as well.

Film thickness

Values of the mean film thickness measured below the feed are plotted in figure 9. The data shown were taken at station *A*, test section configuration II. Values for the Nusselt film thickness are indicated. For the lowest three rates ($Re_F = 310$, 776 and 1552) these are in excellent agreement with measured values below the flooding point. For the highest liquid rate ($Re_F = 3195$) the measured film thickness is in excellent agreement with the theoretical value predicted by Dukler (1960) for turbulent films. Note that the mean film thickness is essentially constant with increasing countercurrent gas flow until just at the flood point. Then two types of changes take place. At low flow rates there is a step *increase* in film thickness. At high rates the liquid film thickness begins to *decrease* at the flood point. These drastically different types of changes at flooding suggest difficult mechanisms control. At the high feed rate the existence of a second transition is displayed at a higher gas rate where the film thickness shows an increase. This corresponds to the two transitions identified in the pressure gradient curves.

Values of the mean film thickness above the feed appear in figure 10. Film thickness is seen to be independent of feed location, to be a maximum just at the conditions of transition and to decrease with increasing shear.

Of particular interest is information on the maximum film thickness. Each digitized time trace was searched for the 5 largest single values of film thickness and these were

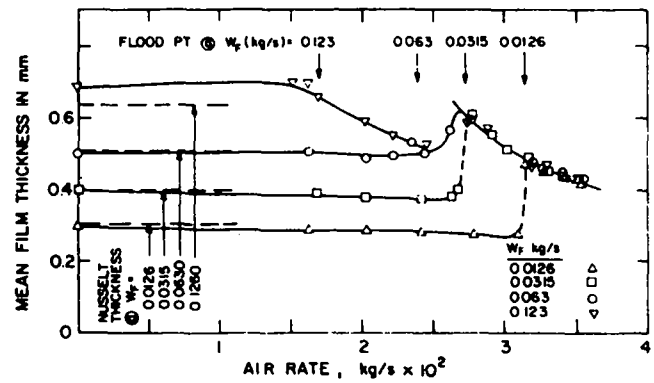

Figure 9. Mean film thickness below the feed (station A, test section II).

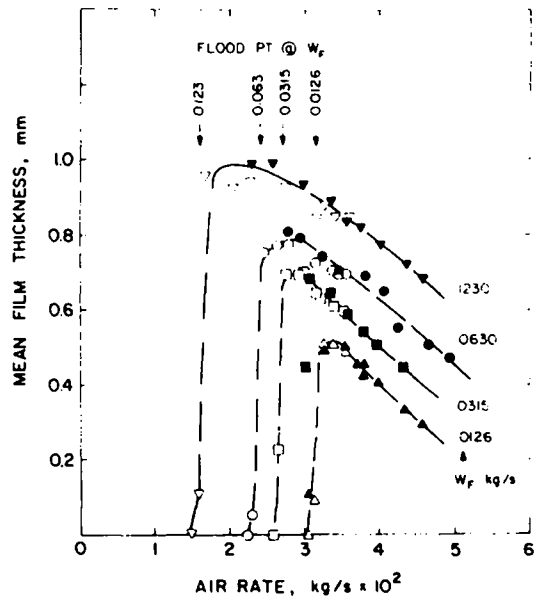

Figure 10. Mean film thickness above the feed (open symbols = station D, test section II, closed symbols = station C, test section III).

averaged to obtain the values shown in figure 11 for below the feed and figure 12 for above the feed. Because visual observations of flooding are so deceptive, it is important to note that under no condition does the maximum thickness approach the radius of the pipe. Despite the fact that bridging has been reported to take place during flooding, in no case is the maximum film thickness below the feed greater than 10% of the radius. Observers have also suggested that when flooding first takes place the liquid rises above the feed as in slugs. However, the data of figure 12 show the film thickness there never exceeds 15% of the radius. While the mean film thickness below the feed remains essentially unchanged until the gas rate at flooding is reached, the maximum film thickness begins to show major changes well below this flood point. In fact, the data suggest the existence of peak values at gas rates 15–20% below the flooding rate. Thus, it seems that significant changes in film structure are precursors to the flooding state and this takes place at gas rates below

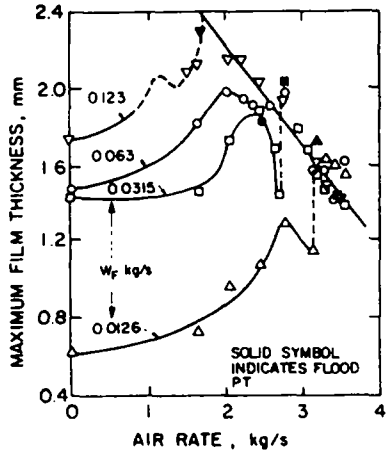

Figure 11

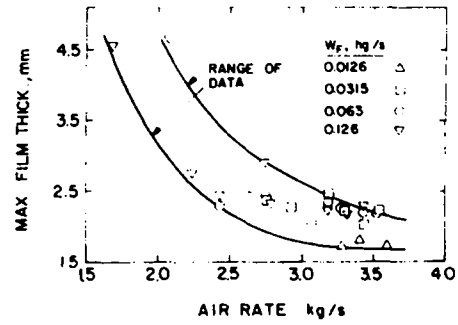

Figure 12

Figure 11. Maximum film thickness measured below the feed (station A, test section II).
Figure 12. Maximum film thickness measured above the feed (station D; test section II).

flooding. Despite these changes in structure below flooding, the pressure gradient and shear are unaffected (figure 7). The conductance probe method becomes less accurate for the measurement of the maximum film thickness values. Very recent measurements in this laboratory using methods with linear response suggest the values in figures 11 and 12 may be understated by 20–40%. However, the conclusion that bridging does not occur remains unchanges.

Other evidence on the change in wave structure below flooding can be deduced from values of RMS film thickness variation calculated from the digitized time series. This quantity, defined as

$$\delta_{RMS} = [(\delta(t) - <\delta>)^2]^{1/2}$$

where $<\delta>$ is the time average film thickness, is shown in figure 13 below the feed and figure 14 for above the feed. Again it is clear that evidence for a coming flooding condition is anticipated by increases in RMS fluctuating film thickness at gas rates well below the flood point. Near flooding there is a dramatic increase in δ_{RMS} even though the mean thickness remains near constant. The curve of δ_{RMS} versus gas rate along the flooding curve is displaced between the low and high rates, giving further evidence for two different mechanisms of flooding.

Probability density distribution data on film thickness also suggest two different flooding mechanisms for high and low rates. Figure 15 for the lowest liquid rate shows the probability density of the free falling film (A), the density at a gas rate just below the gas rate at flooding (B) and at the flood point C. The shift to a much broader distribution at flooding is evident. In contrast, for the highest liquid rate (figure 16) the shift is to smaller film thickness values. Above the feed the density distribution narrows with increasing rate as shown by some examples in figure 17. The data for figures 15–17 were taken in test section configuration II, measuring station C (see figure 1).

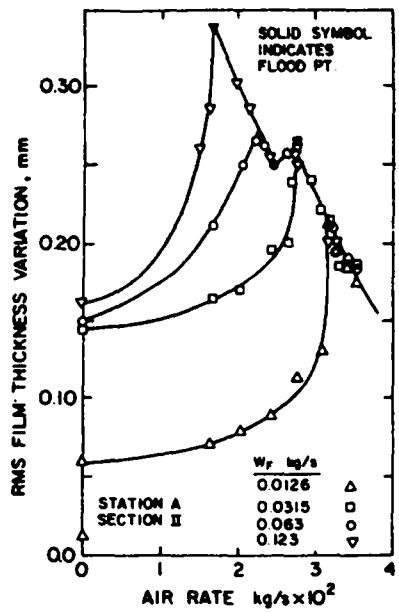

Figure 13

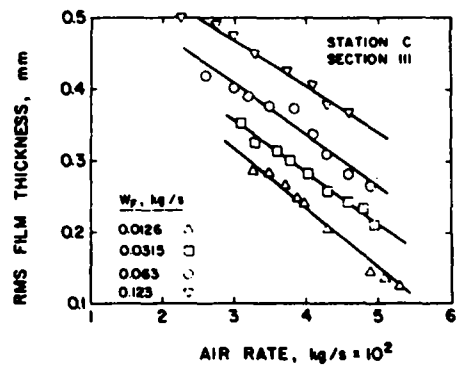

Figure 14

Figure 13. RMS fluctuation in film thickness measured below the feed.
Figure 14. RMS fluctuation in film thickness measured above the feed.

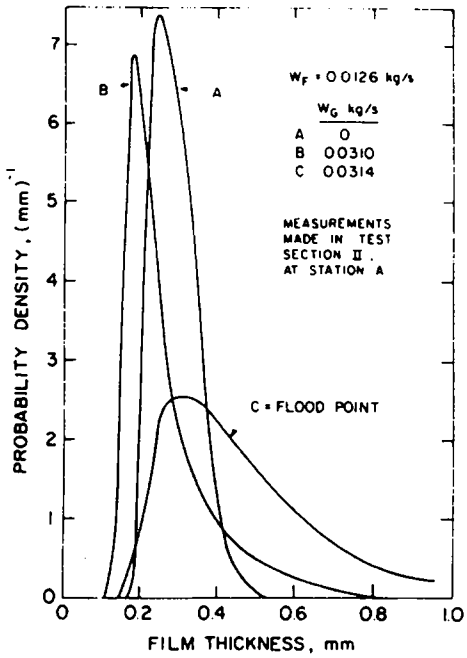

Figure 15

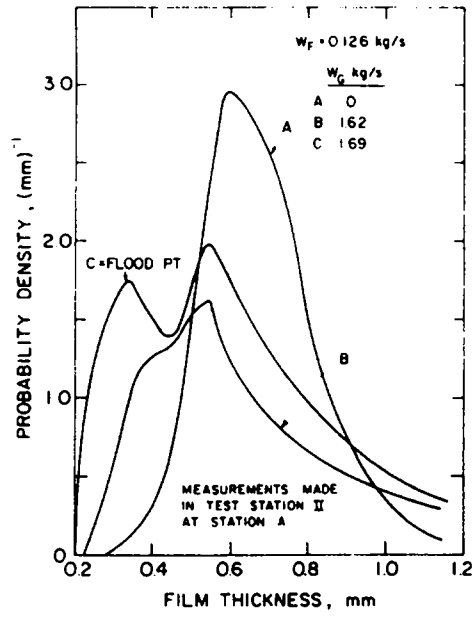

Figure 16

Figure 15. Probability density of film thickness below the feed; $W_F = 0.0126$.

Figure 16. Probability density of film thickness below the feed; $W_F = 0.126$.

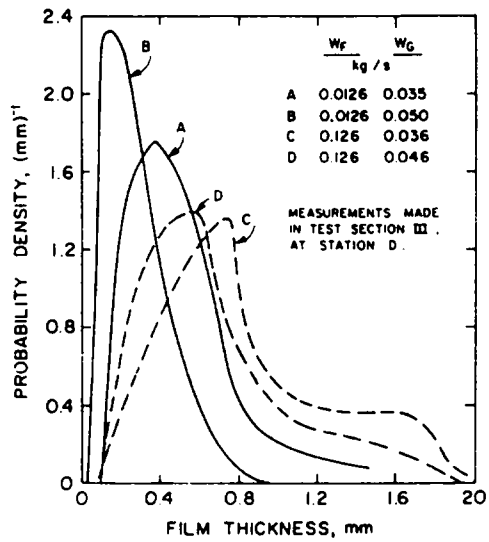

Figure 17. Probability density of film thickness above the feed for two liquid rates.

Friction factor coefficients

The friction factor at the interface f_i was calculated from

$$f_i = \frac{2\tau_i}{\rho_G(\bar{U}_G - \bar{U}_L)^2} \qquad [1]$$

with τ_i evaluated from

$$\tau_i = -\frac{\Delta P}{\Delta L}\left[\frac{D - 2\langle\delta\rangle}{4}\right] \qquad [2]$$

where $\Delta P/\Delta L$ is the pressure gradient and the average liquid and gas velocities from

$$\bar{U}_L = \frac{W_D}{\rho_L \pi \langle \delta \rangle (D - \langle \delta \rangle)} \quad [3A]$$

where the mass rate of liquid flowing down in the film W_D is the measured flow rate in the film.

$$\bar{U}_G = \frac{4W_A}{\rho_G \pi (D - 2\langle \delta \rangle)^2} \quad [3B]$$

where W_A is the mass rate of gas flow, D is the tube diameter, ρ_G and ρ_L are the densities of the gas and liquid. With these data all the information necessary to make these calculations is available.

Wallis (1969) suggested that for liquid films the interfacial friction factor is uniquely related to the ratio of the film thickness to tube diameter. One could expect a correlation of that form if the waves presented a "fully rough" surface to the moving gas stream and, in addition, the roughness height was proportional to film thickness and independent of gas flow rate. A plot of f_i vs δ/D calculated from data taken above the feed appears in figure 18. Indeed, except for the highest flow rate condition where the data scatter somewhat, a single curve does appear to describe the results. The curve is quite different from that suggested by Wallis (1969)

$$f_i = 0.005\left[1 + 300\frac{\langle \delta \rangle}{D}\right].$$

Bharathan (1978) recently measured the pressure gradient using an air–water system and a 5.1 cm dia. pipe. He made an empirical fit to his data and suggested

$$f_i = 0.005 + 406\left(\frac{\langle \delta \rangle}{D}\right)^{2.04} \quad [4]$$

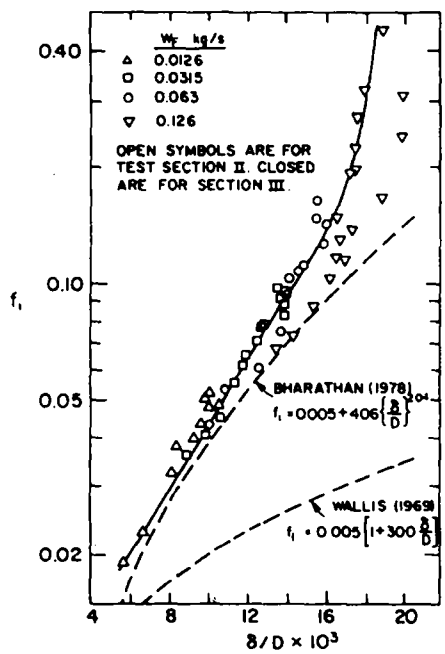

Figure 18. Interfacial friction factor vs δ/D for concurrent upflow above the feed.

The coefficient and exponent changed with pipe size. It is likely to be different for other fluid properties as well. As expected, because of similarity of conditions of the experiment, [4] shows reasonable agreement with the data presented here.

A rather different view of interfacial friction factor dependence appears in figure 19. The suggested unique relationship between f_i and (δ/D) is based on the premise that the surface is fully rough. For this condition the friction factor becomes constant for each roughness and independent of gas phase Reynolds number. The data as plotted in figure 19 suggest a different interpretation. In fact, it would appear that the interface behaves as a transitionally rough surface where the friction factor depends both on the roughness *and* Re_G where

$$\mathrm{Re}_G = \frac{4W_A}{\pi(D - 2\langle\delta\rangle)\mu_G} \qquad [5]$$

where W_A is the gas mass rate of flow and μ_G is its viscosity. It would appear that the premise that f_i depends only on δ/D has only limited general validity.

In the calculation of film behavior friction factor at the wall is of interest. This quantity can be calculated from the data by means of a force balance on the flowing stream.

$$\tau_w = \frac{\Delta P}{\Delta L}\frac{D}{4} - \rho_L g(D - \langle\delta\rangle)\frac{\langle\delta\rangle}{D} - \rho_G g\frac{(D - 2\langle\delta\rangle)^2}{4D} \qquad [6]$$

where positive values of τ_w designate downward directed shear. $\Delta P/\Delta L$ is the measured pressure gradient while ρ_L and ρ_G are the liquid and gas densities. All quantities on the right-hand side in [6] are measured. The wall friction factor is defined as

$$f_w = \frac{2\tau_w}{\rho_L \bar{U}_L^2} \qquad [7]$$

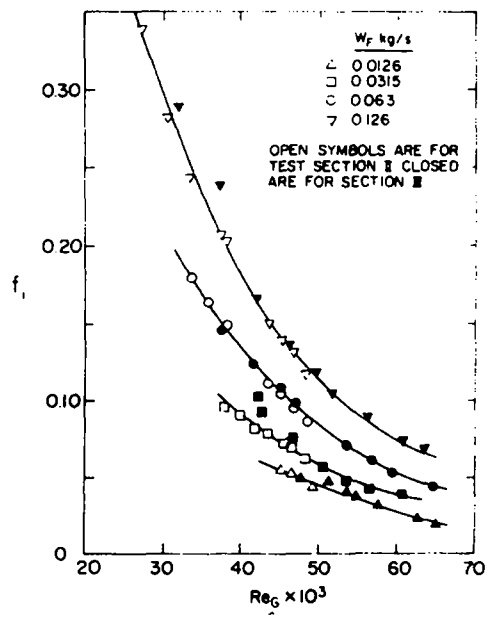

Figure 19. Interfacial friction factor–Reynold number relation for concurrent upflow above the feed.

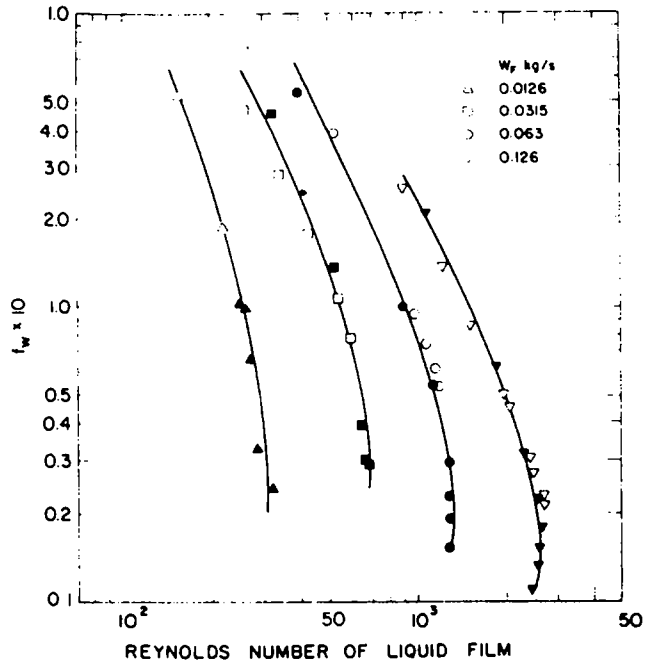

Figure 20. Wall friction factor for upflow (open symbols are for test section II, closed for III).

and the liquid film Reynolds number by

$$\mathrm{Re}_D = \frac{4W_D}{\pi D \mu_L}. \qquad [8]$$

The experimental data calculated to these coordinates are shown in figure 20. Bharathan (1978) and Wallis (1969) have suggested a value of $f_w = 0.005$. Clearly this does not describe the experimental results.

Acknowledgement—The financial support of the U.S. Nuclear Regulatory Commission for this research is gratefully acknowledged.

REFERENCES

BHARATHAN, D. 1978 Air–water countercurrent annular flow in vertical tubes. *Electric Power Research Institute Report, EPRI NP-786.*

CHOPRA, A. 1982 Characteristics and modelling of annular two phase flows. PhD Dissertation, Univ. of Houston.

CHU, K. J. & DUKLER, A. E. 1974 Statistical characteristics of thin wavy films—II. Studies of the substrate and its wave structure. *AIChE J.* **20**, 695–706.

DUKLER, A. E. 1960 Fluid mechanics and heat transfer in vertical falling film systems. *Chem. Engng. Prog. Symp. Ser.* **56**, 1–10.

DUKLER, A. E. & SMITH, L. 1977 Two phase interactions in countercurrent flow: studies of the flooding mechanism. *U.S. Nuclear Regulatory Commission Report, NUREG/CR-0617.*

GAZLEY, C. 1948 Interfacial shear and stability in two phase flow. Ph.D. Thesis, Univ. of Delaware.

SMITH, L. 1983 Flooding phenomena. MS Thesis, Univ. of Houston.

TIEN, C. L., & LIU, C. P. 1979 Survey on vertical two phase countercurrent flooding. *Electric Power Research Institute Report NP-984.*

WALLIS, G. 1969 *One Dimensional Two Phase Flow.* McGraw-Hill, New York.